

Strain relaxation of SiGe islands on compliant oxide

H. Yin^{a)}

Center for Photonics and Optoelectronic Materials and Department of Electrical Engineering, Princeton University, Princeton, New Jersey 08544

R. Huang

Princeton Materials Institute and Department of Civil and Environmental Engineering, Princeton University, Princeton, New Jersey 08544

K. D. Hobart

Naval Research Laboratory, Washington, DC 20375

Z. Suo

Princeton Materials Institute and Department of Mechanical and Aerospace Engineering, Princeton University, Princeton, New Jersey 08544

T. S. Kuan and C. K. Inoki

Department of Physics, University at Albany, State University of New York, Albany, New York 12222

S. R. Shieh and T. S. Duffy

Department of Geosciences, Princeton University, Princeton, New Jersey 08544

F. J. Kub

Naval Research Laboratory, Washington, DC 20375

J. C. Sturm

Center for Photonics and Optoelectronic Materials and Department of Electrical Engineering, Princeton University, Princeton, New Jersey 08544

(Received 20 December 2001; accepted for publication 29 March 2002)

The relaxation of patterned, compressively strained, epitaxial $\text{Si}_{0.7}\text{Ge}_{0.3}$ films transferred to borophosphosilicate (BPSG) glass by a wafer-bonding and etch-back technique was studied as an approach for fabricating defect-free $\text{Si}_{1-x}\text{Ge}_x$ relaxed films. Both the desired in-plane expansion and undesired buckling of the films concurrently contribute to the relaxation. Their relative role in the relaxation process was examined experimentally and by modeling. Using x-ray diffraction, Raman scattering and atomic force microscopy, the dynamics of in-plane expansion and buckling of $\text{Si}_{0.7}\text{Ge}_{0.3}$ islands for island sizes ranging from $10\ \mu\text{m} \times 10\ \mu\text{m}$ to $200\ \mu\text{m} \times 200\ \mu\text{m}$ for anneal temperatures between 750 and 800 °C was investigated. Lateral relaxation is favored in small and thick islands, and buckling is initially dominant in large and thin islands. Raising the temperature to lower viscosity of the oxide enhances the rate of both processes equally. For very long annealing times, however, the buckling disappeared, allowing larger, flat, and relaxed islands to be achieved. Cross-sectional transmission electron microscopy observation on a relaxed $\text{Si}_{0.70}\text{Ge}_{0.30}$ island revealed no dislocations, confirming that SiGe relaxation on BPSG is a good approach to achieve high quality relaxed SiGe. © 2002 American Institute of Physics. [DOI: 10.1063/1.1479757]

I. INTRODUCTION

Compliant substrates have been under intensive study since the concept¹ was proposed in 1991 as a means to achieve high quality epitaxial thin films in cases where lattice matched substrates are not available. The underlying physical principle of a compliant substrate is to utilize the compliance of the substrate to release the misfit strain in a thin film on top of it without the generation of dislocations. There have been various ways to realize compliant substrates, including wafer bonding,² glass transformation through ion implantation³ and other methods.^{4,5} For various silicon-based heterostructural devices, a substrate template

for subsequent epitaxy is often desired with a lattice constant between that of silicon and germanium. One approach towards achieving such layers involves growing graded epitaxial mismatched structures directly on silicon substrates.⁶ This process requires the creation of misfit dislocations, which causes unwanted threading dislocations in the top relaxed $\text{Si}_{1-x}\text{Ge}_x$ layer. To create defect-free $\text{Si}_{1-x}\text{Ge}_x$ layers, Hobart *et al.*² studied the relaxation of laterally compressed SiGe islands transferred to a viscous borophosphosilicate (BPSG) compliant film. That work showed that small islands relaxed as desired, but large islands became rough because of an undesired buckling process (Fig. 1). This article uses experimentation and modeling to quantitatively examine this problem and demonstrate possible solutions to create large smooth islands.

^{a)}Electronic mail: hyin@ee.princeton.edu

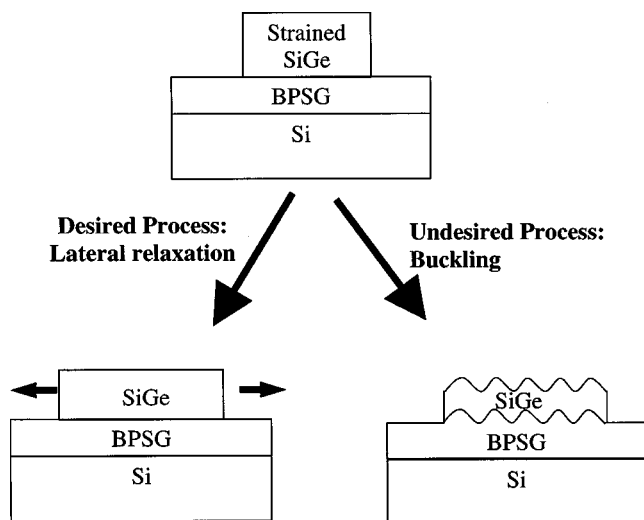


FIG. 1. Diagram of relaxation mechanisms: lateral relaxation vs buckling. The SiGe film follows the BPSG profile.

II. EXPERIMENTAL PROCEDURE AND CHARACTERIZATION

The basic fabrication process is the same as that of Ref. 2. The host wafer is a silicon wafer on which 30 nm commensurately strained $\text{Si}_{0.70}\text{Ge}_{0.30}$ is grown followed by 2 nm Si cap. The host wafer was implanted with H_2^+ at an ion energy of 180 keV and a dose of $4.5 \times 10^{16} \text{ cm}^{-2}$. The handle wafer is a silicon wafer coated with 200 nm BPSG (4.4% B and 4.1% P by weight). The wafers were cleaned and bonded at room temperature. The wafer pair was annealed at 250 °C for 4 h to enhance bond strength and then at 550 °C in N_2 ambient to separate the top layer from the host substrate at the depth of the hydrogen implant. The remaining silicon on top of the SiGe was removed by selective etching to leave ~30 nm compressively strained $\text{Si}_{0.70}\text{Ge}_{0.30}$ on the BPSG. Due to native oxide formation and interdiffusion with the SiGe, the thickness of Si in the final SiGe/Si/BPSG structure is less than its original thickness of 2 nm (negligible compared with 30 nm SiGe), and, consequently, its existence is ignored when the mechanical behavior of this structure is analyzed.

The continuous $\text{Si}_{0.70}\text{Ge}_{0.30}$ film on those samples is patterned into arrays of square islands of various sizes from 10 to 200 μm by reactive ion etch. X-ray diffraction (XRD) was carried out on arrays of identical islands to measure the vertical strain of $\text{Si}_{0.70}\text{Ge}_{0.30}$ on BPSG before and after annealing. When the SiGe film roughens, SiGe XRD peak will vanish because the Bragg condition can no longer be satisfied simultaneously by the entire film. A pair of (004) rocking curves are used to extract the perpendicular lattice constant a_{\perp} . We expect that the SiGe film is commensurately strained without misfit dislocations within it, so the perpendicular lattice constant is expected to be the same throughout the depth of the SiGe. Due to the nonuniform strain across islands, the spatially averaged perpendicular lattice constant across an island measured by XRD is

$$a_{\perp}(\text{average}) = \frac{1}{\text{Area}_{\text{island}}} \int_{\text{Island}} a_{\perp}(x,y) dx dy. \quad (1)$$

The error of the SiGe XRD peak position of SiGe on BPSG, introduced by misalignment of the SiGe vertical crystalline orientation with respect to that of the Si substrate, is removed by averaging two measurements in which samples were rotated by 180°. The in-plane lattice constant a_{\parallel} is calculated from⁷

$$a_{\perp} - a_r = -2(c_{12}/c_{11})(a_{\parallel} - a_r), \quad (2)$$

where a_r is the fully relaxed lattice constant, and c_{12} and c_{11} are its elastic constants.⁸ The strain fraction s is defined as follows:

$$s = (a_r - a_{\parallel}) / (a_r - a_{\text{Si}}), \quad (3)$$

where a_{Si} is the lattice constant of Si.⁸

Raman spectroscopy was used to locally probe the strain in the SiGe film. An Ar^+ laser (514.5 nm) was focused using a microscope objective to a diameter of ~3 μm on the sample surface. The Raman frequency shift due to the Si-Si optical phonon mode in the SiGe film was measured with an accuracy of $\pm 0.5 \text{ cm}^{-1}$. The phonon energy (and thus Raman shift) depends on both the strain and the Ge fraction,⁹ but there are significant discrepancies in published strain-shift coefficients.¹⁰ The strain-shift coefficients for phonons in $\text{Si}_{1-x}\text{Ge}_x$ epi-layers are strong functions of Ge content.⁹ The Si-Si phonon frequencies of the fully strained and fully relaxed $\text{Si}_{0.70}\text{Ge}_{0.30}$, verified by XRD, were found to be 512 and 503 cm^{-1} , respectively. The error in the Ge fraction is estimated to be $\pm 1\%$. Assuming a biaxial strain in the as-grown $\text{Si}_{0.70}\text{Ge}_{0.30}$ (Ge content determined by XRD) the following relation was used to relate the Raman shift and the local biaxial strain:

$$\omega_{\text{Si-Si}} = 512 \text{ cm}^{-1} - 750\epsilon \text{ cm}^{-1}, \quad (4)$$

where $\omega_{\text{Si-Si}}$ is the frequency of Si-Si phonons and ϵ is the strain of the film.

The surface roughness of SiGe films was measured by atomic force microscopy (AFM) and the root of mean square (rms) of the surface profile was used to characterize the surface morphology. Cross sectional transmission electron microscopy (XTEM) was also employed to characterize films after relaxation.

III. RESULTS AND DISCUSSION

A. Qualitative trends

Islands of $\text{Si}_{0.70}\text{Ge}_{0.30}$ on BPSG were annealed under various conditions to examine the rates of in-plane expansion and buckling (Fig. 1). In-plane expansion happens first on the edge of islands and propagates towards the center. Therefore, the smaller the islands are, the faster in-plane expansion reaches the center. On the other hand, the buckling mechanism is not a boundary effect and, consequently, independent of island size. Figure 2 shows an optical micrograph of a corner of a 100 $\mu\text{m} \times 100 \mu\text{m}$ island after 90 min anneal at 790 °C. It shows three distinct relaxation regions: (1) buckling is entirely avoided in the corner close to the edge where

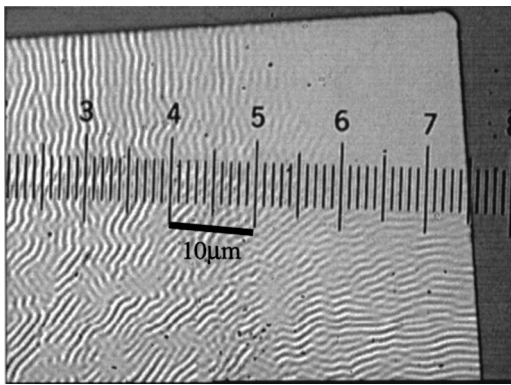


FIG. 2. Optical micrograph of a corner of $100\ \mu\text{m}\times 100\ \mu\text{m}$ $\text{Si}_{0.7}\text{Ge}_{0.3}$ island after a 90 min annealing at $790\ ^\circ\text{C}$ in nitrogen.

in-plane expansion takes place quickly to relax strain, (2) buckling appears in areas where in-plane expansion only releases strain along one direction, i.e., normal to the edge, and (3) in the island center where strain is only relaxed by buckling. Figure 3 summarizes the relaxation behavior as a function of island sizes. Small islands relax quickly before buckling can occur and remain flat (Fig. 3). For large islands (e.g., larger than $80\ \mu\text{m}\times 80\ \mu\text{m}$), the in-plane relaxation is negligible in the center of islands and the buckling approaches a maximum level. Figure 4 shows the strain distribution measured by Raman spectroscopy across a $60\ \mu\text{m}\times 60\ \mu\text{m}$ island along the diagonal direction, which clearly shows that the strain relaxes first on the boundary and the relaxation propagates towards the center. Note the data and model of Fig. 4 represent the local strain, so that integrating this quantity over the island gives the average strain [e.g., as measured by XRD using Eq. (1)]. The next two sections study the lateral and buckling processes, respectively. In the last section, they are combined to examine how the desired in-plane expansion process can be enhanced.

B. Quantitative study of lateral relaxation

The goal of this section is to quantitatively understand the lateral relaxation. The one-dimensional (1D) model of the lateral relaxation of strained islands on a viscous layer was studied by different groups.^{11,12} Recently Huang *et al.*¹³ have developed a generalized model for the two-dimensional

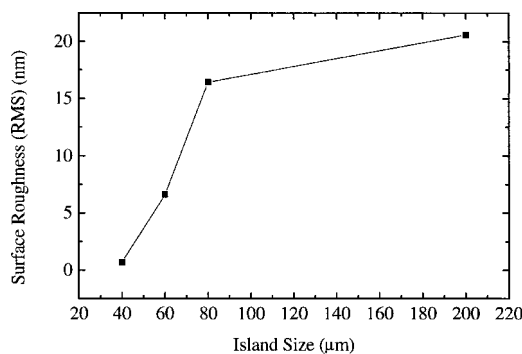


FIG. 3. Surface roughness at the center of islands of various sizes after a 90 min annealing at $790\ ^\circ\text{C}$ in nitrogen.

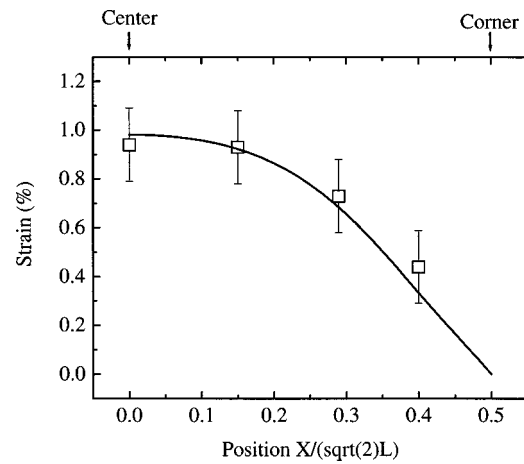


FIG. 4. Strain distribution along the diagonal of a $60\ \mu\text{m}\times 60\ \mu\text{m}$ island after a 17 min annealing at $790\ ^\circ\text{C}$. Open squares are experimental data and the solid line is the fitting based on the 2D lateral expansion theory (see Ref. 13). The surface roughness rms of the island center is about 1 nm due to buckling, whose contribution to strain relaxation is negligible. L denotes island edge length, which is $60\ \mu\text{m}$ in this case.

(2D) case for square islands and found that the time scale of the lateral relaxation is the same as that of the 1D model

$$\tau_L = \frac{\eta L^2}{c_{11} h_f h_g} \quad (5)$$

L is the island edge length, η is the viscosity of the glass, h_g is the thickness of the glass, and c_{11} and h_f are the elastic coefficient and thickness of the $\text{Si}_{0.7}\text{Ge}_{0.3}$ film, respectively. Vertical island edges were assumed, but given the large island size ($10\text{--}200\ \mu\text{m}$) compared to the island thickness of only $\sim 30\ \text{nm}$, the exact shape of the edge is not critical. As shown in Fig. 5, small islands relax considerably faster than large islands, as predicted by Eq. (5). Since the data in Fig. 5 were obtained by XRD on arrays of islands, the measured strain is spatially averaged across islands. For large islands, the surface tends to roughen by buckling after a long time anneal, and accordingly, the XRD peaks of large SiGe islands broaden and vanish. This accounts for the disappearance of XRD peaks of 30 and $40\ \mu\text{m}$ islands for annealing times longer than 20 min at $790\ ^\circ\text{C}$. To demonstrate that the

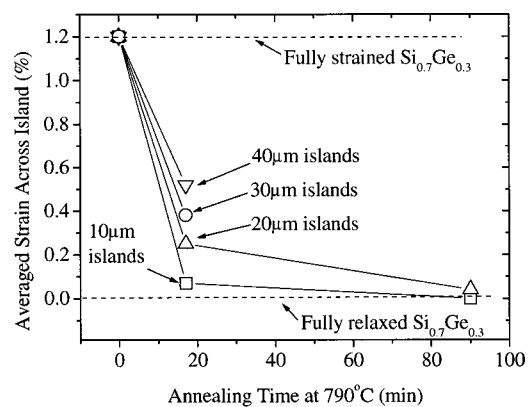


FIG. 5. Averaged strain across islands (measured by XRD) vs annealing time at $790\ ^\circ\text{C}$ in nitrogen.

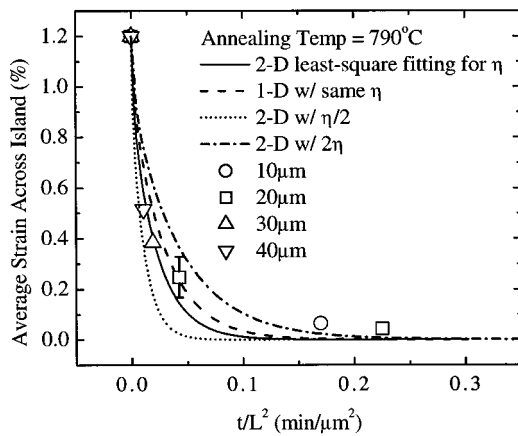
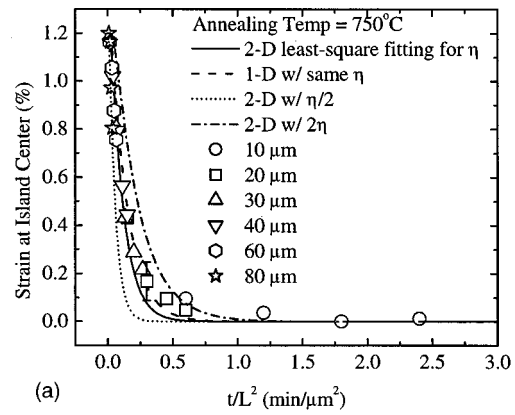


FIG. 6. Averaged strain across islands, measured by XRD, as a function of normalized annealing time at 790 °C for island sizes from 10 to 40 μm. Open symbols are experimental data. The error bar of the experimental data is ±0.075%, as shown on one data point. Least-square fitting based on the 2D model gives rise to the solid line with the only fitting parameter viscosity to be 1.3×10^{10} N s/m². The dashed line is the 1D model using the same viscosity. The short-dot line and the dash-dot line reflect the 2D model with half and twice, respectively, of the extracted viscosity to show the fit sensitivity to the viscosity.

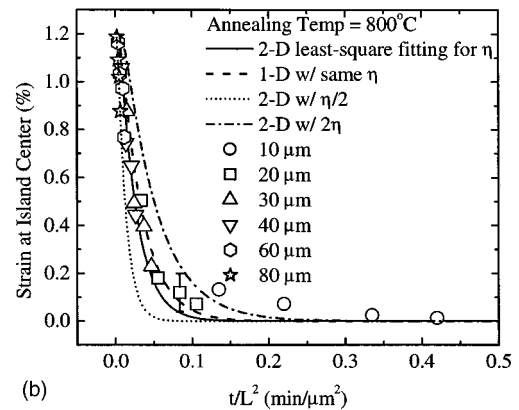
lateral relaxation indeed quantitatively scales as predicted by Eq. (5), the data of Fig. 5 have been replotted by normalizing the time axis for each island size (Fig. 6). The prediction of the 2D model, using a least-square fit to all data points and using viscosity as a single fitting parameter (1.3×10^{10} N s/m²), is also shown, along with the 1D model using the same viscosity. The difference between the 1D and 2D models is small, within the error bar of the experimental data. Table I lists the values used for the mechanical properties and the physical structure. All data points fall on a single curve as expected.

Figure 7 shows the strain at the island center, measured by Raman scattering, over time for islands of various sizes at 750 and 800 °C. The strain at the island center is slower to relax than the averaged strain. Again, the viscosity value is extracted by fitting data to the 2D model, with resulting values of 5.5×10^{10} N s/m² at 750 °C and 1.2×10^{10} N s/m² at 800 °C.

Note that the viscosity is higher than that estimated solely based on the composition of the BPSG film ($1-3 \times 10^8$ N s/m² at 800 °C for a glass with 4.4% B and 4.1% P by weight).² This could be due to uncertainty in the BPSG composition, an uncertainty in the relationships between composition and viscosity and/or viscosity and temperature, or an unknown enhancement of viscosity in very thin films. Nevertheless, this section demonstrates that we can quantitatively model the average lateral island relaxation as well as the profile of the relaxation across the island.



(a)



(b)

FIG. 7. Strain at the island center, measured by Raman scattering, as a function of normalized anneal time at (a) 750 °C and (b) 800 °C for island size from 10 to 80 μm. Open symbols are experimental data. The error bar of the experimental data is ±0.075%, as shown on one data point. Least-square fitting based on the 2D model gives rise to the solid line with the only fitting parameter viscosity to 5.5×10^{10} N s/m² (750 °C) and 1.2×10^{10} N s/m² (800 °C). The dashed line is the 1D model using the same viscosity. The short-dot line and the dash-dot line reflect the 2D model with half and twice, respectively, of the extracted viscosity to show the fit sensitivity to the viscosity.

C. Quantitative study of buckling

We now address the issue of buckling. The theory of buckling of a continuous film on a viscous layer has been first developed by Sridhar, Srolovitz, and Suo¹⁴ and then refined by Huang and Suo^{15,16} and Sridhar, Srolovitz, and Cox.¹⁷ Surface buckling is a superposition of many exponentially growing modes. Each mode is a sinusoidal surface profile, whose amplitude rises exponentially over time¹⁴

$$A(t) = A_0 e^{t/\tau_B}, \tag{6}$$

where A is surface roughness, A_0 is the initial surface roughness, and τ_B is the buckling time constant, which is determined by¹⁴

TABLE I. Mechanical properties (see Ref. 8) of SiGe film (linearly interpolated between Si and Ge) and dimensions of the SiGe and BPSG films used in models for lateral relaxation and buckling.

$E(\text{Si}_{0.7}\text{Ge}_{0.3})$ (10^{10} N/m ²)	$C_{11}(\text{Si}_{0.7}\text{Ge}_{0.3})$ (10^{10} N/m ²)	$\nu(\text{Si}_{0.7}\text{Ge}_{0.3})$	$\epsilon_0(\text{Si}_{0.7}\text{Ge}_{0.3})$	$h_g(\text{nm})$	$h_f(\text{nm})$
14.9	15.4	0.279	1.2%	200	30

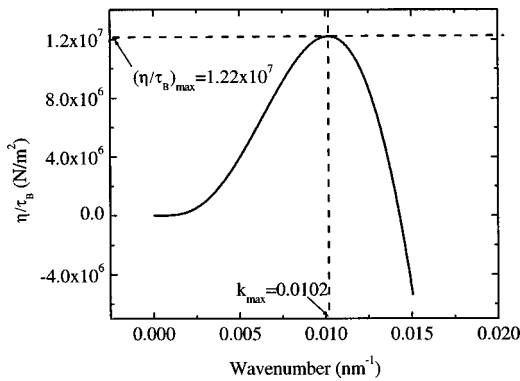


FIG. 8. Product of the viscosity and the inverse of exponential buckling time constant (η/τ_B) as a function of buckling wave number, based on Eq. (7) and parameters in Table I.

$$\frac{1}{\tau_B} = \frac{1}{\eta} \frac{E}{24(1-\nu^2)} \left[\frac{\sinh(2h_g k) - 2h_g k}{1 + \cosh(2h_g k) + 2(h_g k)^2} \right] \times [\beta(h_f k) - (h_f k)^3], \quad (7)$$

where E and ν are the Young's Modulus and Poisson's ratio of the $\text{Si}_{0.70}\text{Ge}_{0.30}$ film, respectively, $\beta = 12\epsilon_0(1 + \nu)$, ϵ_0 is the strain in $\text{Si}_{0.7}\text{Ge}_{0.3}$ and k is the wave number of the mode. Using the parameters in Table I and Eq. (7), the product of viscosity and the inverse of exponential time constant (η/τ_B) as a function of the buckling wave number are plotted in Fig. 8. Due to the exponential growth over time, it is assumed that the fastest growing mode will dominate the final surface topology eventually, which greatly simplifies our comparison between the theory and experiments. This single mode assumption leads to a predicted exponential growth of the surface roughness as long as the buckling does not significantly alter the strain. This model also neglects any reduction of strain from lateral relaxation, so it is valid for an infinite film or near the center of large islands. Therefore, for example, from Fig. 8 we would expect the fastest growing mode with the parameters of Table I (SiGe thickness of 30 nm) to have a wave number of 0.01 nm^{-1} , corresponding to a wavelength of $0.63 \mu\text{m}$.

Figure 9 shows rms surface roughness at the center of $200 \mu\text{m} \times 200 \mu\text{m}$ islands as a function of anneal time, which is expected to be similar to that of a continuous film (Fig. 3). The data represented by open squares (SiGe thickness of 30 nm) are discussed at this point and the other set will be addressed in the next section. The surface roughness at small amplitude grows exponentially with time as predicted. It then saturates as expected for long annealing times because buckling reduces the strain, which is the driving force for the buckling. The buckling exponential time constant can be estimated as follows: Eq. (7) plotted in Fig. 8 predicts the dominant buckling mode has η/τ_B quotient of $1.22 \times 10^7 \text{ N/cm}^2$. The viscosity η was measured in the previous section by the rate of lateral expansion of small islands (where buckling does not significantly contribute to the strain relief) to be $1.3 \times 10^{10} \text{ N s/m}^2$ at 790°C . Combining these two results, τ_B is expected to be $1.1 \times 10^3 \text{ s}$. Using this value of τ_B , the initial phase of the buckling growth for the 30 nm SiGe layer in Fig. 9 was fitted to Eq. (6), with the

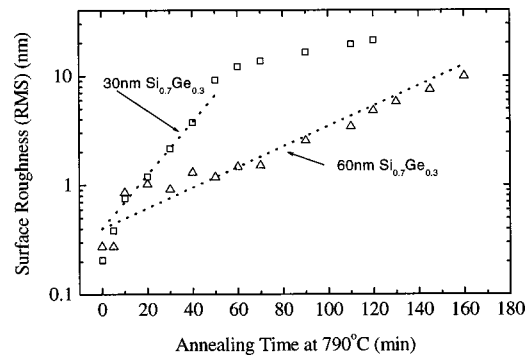


FIG. 9. Surface roughness vs annealing time at 790°C for $\text{Si}_{0.7}\text{Ge}_{0.3}$ of thickness 30 and 60 nm, measured at the center of $200 \mu\text{m} \times 200 \mu\text{m}$ $\text{Si}_{0.70}\text{Ge}_{0.30}$ islands. Open symbols are experimental data and dotted lines are fits to a simple exponential growth, with predetermined buckling time constant of 18 min (30 nm) and 46 min (60 nm), and the initial surface roughness as a single fitting parameter for each curve for the range of small surface roughness.

initial surface roughness A_0 as a single fitting parameter. The resulting fit is excellent. Further, the model predicts a wavelength of $0.63 \mu\text{m}$ for the dominant buckling mode, and a wavelength of approximately $1.0 \mu\text{m}$ is observed. Because of the uncertainty in estimating an average wavelength, it was not possible to discern any change in wavelength versus time.

The excellent agreement between the model and data for both buckling and in-plane expansion gives us high confidence in our understanding of the relaxation processes, enabling us next to explore the case where buckling and lateral relaxation occur simultaneously.

D. Achieving lateral relaxation versus buckling

In this section, the trade-off between the desired lateral relaxation and the undesired buckling is examined using the models developed above for lateral relaxation (Sec. B) and for buckling (Sec. C) as well as experiments. Modeling in this regime where both lateral expansion and buckling are present^{15,18} is more complicated than that above in regimes where only lateral relaxation (small islands) or buckling (large islands) are considered. The cases examined are (i) varying the temperature (and/or the glass viscosity), (ii) increasing the SiGe thickness, and (iii) very long annealing times.

1. Varying temperatures and viscosity

First, the annealing temperature was varied from 750 to 800°C to change the viscosity from 5.5×10^{10} to $1.2 \times 10^{10} \text{ N s/cm}^2$, as measured in Sec. B. The lower viscosity allows a faster lateral relaxation, as expected from Eq. (5) and as observed by comparing the time scale of Figs. 7(a) and 7(b). From Eq. (7), the buckling time constant also is expected to decline as viscosity is decreased. Both time constants scale similarly with viscosity, namely to the first power. Therefore, one expects lowering the viscosity (either by temperature or by changing the glass composition) will increase the rate of both processes equally, but not favor one over the other. This is supported experimentally: the evolution of surface roughness versus strain in the center of the

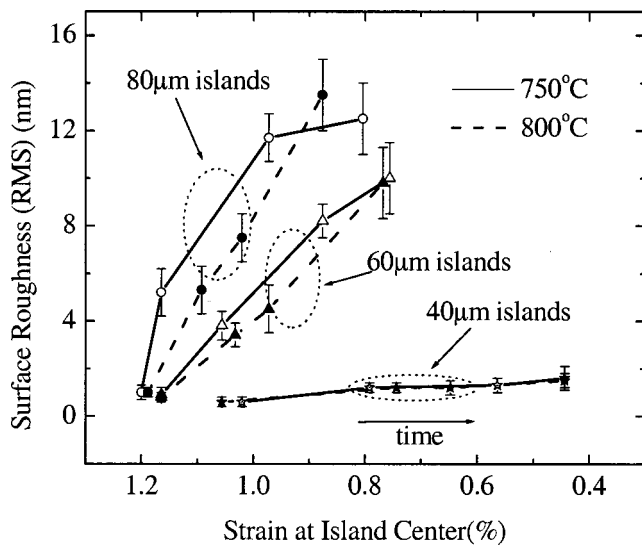


FIG. 10. Evolution of surface roughness vs strain at the center of islands at 750 and 800 °C for 40, 60 and 80 μm islands. The longest anneal time at 750 and 800 °C is 240 and 40 min, respectively.

islands is indistinguishable for 750 and 800 °C for each island size as annealing progresses (Fig. 10). For all island sizes, as the sample is annealed the strain decreases and the surface roughness increases. Large islands roughen more than small islands for the same amount of relaxation. Most significantly, although the points plotted represent very different time spans at 750 and 800 °C (240 vs 40 min, respectively) the evolution of roughness versus strain is very similar. Therefore, simply changing the viscosity does not solve the buckling problem.

2. SiGe thickness

Equation (5) predicts a faster lateral relaxation for thicker SiGe layers, as a thicker strained layer exerts more stress on the BPSG layer. A thicker SiGe layer is also expected to have a larger buckling time constant because the SiGe layer is stiffer. For example, Eq. (7) predicts that raising the SiGe thickness from 30 to 60 nm should increase the buckling time constant by a factor of 2.6. More sophisticated modeling supports these trends of preferred lateral relaxation versus buckling for thick islands.¹⁸

Experimentally, it is difficult to increase the original SiGe strained layer thickness because of the critical thickness constraint. Therefore, after a 30 nm Si_{0.70}Ge_{0.30} layer was transferred to the BPSG and the original substrate was removed, a further layer of 30 nm Si_{0.70}Ge_{0.30} commensurately strained film was grown by rapid thermal chemical vapor deposition on the existing fully strained 30 nm Si_{0.70}Ge_{0.30}/BPSG, making the total thickness of Si_{0.7}Ge_{0.3} 60 nm. A short low temperature (800 °C) hydrogen bake was able to remove the native oxide before growth without contributing to relaxation or buckling.¹⁹ The growth temperature was 625 °C, low enough to avoid any glass flow during the growth. Relaxation is negligible at temperature lower than 700 °C.² This structure was then annealed at 790 °C and the time dependence of the surface roughness (rms) at the center of 200 μm × 200 μm islands was measured (see open triangles in Fig. 9). The buckling growth of the 60 nm SiGe

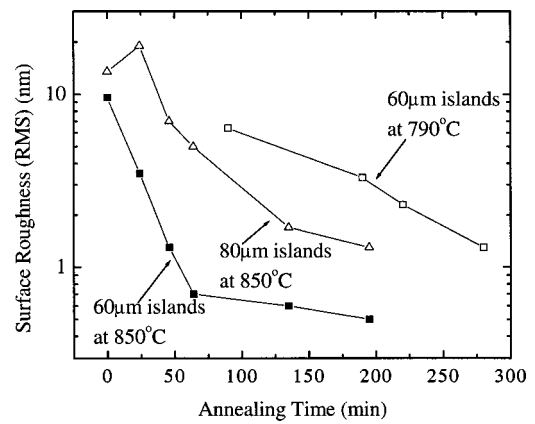


FIG. 11. Surface roughness as a function of annealing time at island center for 60 and 80 μm islands at 790 and 850 °C for Si_{0.70}Ge_{0.30} thickness of 30 nm. Samples annealed at 850 °C initially have a buckled Si_{0.70}Ge_{0.30} surface because they first went through an annealing of 35 min at 800 °C.

film is clearly much slower than the 30 nm SiGe film, as predicted. This was quantitatively modeled with Eq. (7) as in the 30 nm SiGe case by using the viscosity of 1.3×10^{10} N s/m² and a single fitting parameter A_0 (initial buckling amplitude) of 0.4 nm. Again a good fit is obtained. It turns out that the 30 nm film and the 60 nm film have the same fitted initial surface roughness of 0.4 nm, which implies that the surface roughness before annealing is the same for both the 30 and 60 nm SiGe films.

3. Long annealing times

A third approach to achieve flat relaxed SiGe islands is to anneal buckled islands for very long times. The buckled film is not a minimum energy state because of the strain energy stored in the buckled film. Lateral expansion is expected to smoothen surface roughness because it releases this strain energy. Therefore, annealing islands for a long time allow lateral expansion to reach the island center and should subsequently flatten entire islands. Figure 11 shows surface roughness at the center of islands of various sizes for annealing at 790 and 850 °C. The buckling of 60 μm islands after 100 min at 790 °C was 6 nm, which decreased to ~1.3 nm after 280 min at 790 °C. This reduction in surface roughness can be dramatically improved by higher temperature and lower viscosity: at 850 °C the buckling at the center of 60 μm islands is reduced to 0.7 nm after 64 min, and to ~1.3 nm after 195 min on 80 μm islands.

Therefore, buckling grows for short time scales, when lateral expansion is slow, and then decreases at large time scales, when lateral expansion reaches the island center. Qualitatively, the curves of surface roughness versus strain (Fig. 10) will eventually turn over and come down.

E. TEM analysis

XTEM was carried out on a similar Si_{0.7}Ge_{0.3}/Si/BPSG structure to those used in the above experiments. In this sample, thickness of Si_{0.70}Ge_{0.30}, Si and BPSG is 30, 4, and 240 nm (vs 30, 2, and 200 nm in the above experiments), respectively. It was patterned into 40 μm × 40 μm islands and then annealed at 825 °C for 90 min. XRD data confirm that the islands are fully relaxed after this annealing. Figure

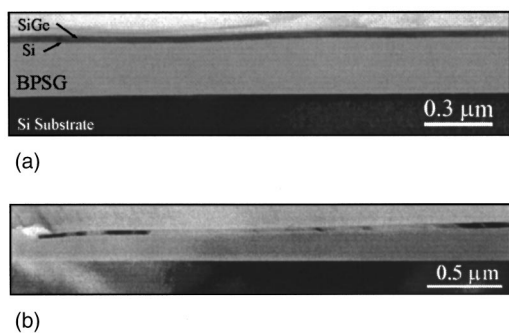


FIG. 12. XTEM of a part of a $40\ \mu\text{m}\times 40\ \mu\text{m}$ island of $\text{Si}_{0.7}\text{Ge}_{0.3}$ (30 nm)/Si (4 nm) on BPSG after 90 min at $820\ ^\circ\text{C}$: (a) island center and (b) island edge. The alternating contrast in the SiGe layer is due to bending of the SiGe film.

12 shows both the center and edge of the island after relaxation. No dislocations are observed in the small area that was probed, but a small undulation due to residual buckling exists throughout the island, with a wavelength of $3\ \mu\text{m}$ and rms amplitude of $\sim 3\ \text{nm}$. It is unlikely that this undulation was caused by TEM sample preparation, since undulations of the same order of magnitude have been observed in similar samples measured by AFM. Note, at the edge of the island the SiGe film bends down slightly with thinner BPSG. We expect that this may be due to the lateral expansion of the island edge during relaxation. The electron diffraction pattern indicates exact in-plane lattice match between the 4 nm Si and 30 nm $\text{Si}_{0.7}\text{Ge}_{0.3}$ layers after annealing (Fig. 13). The vertical streaks in the diffraction pattern show that the very thin Si film is now under tension. The lack of streaks in the horizontal direction indicates that the parallel lattice constant

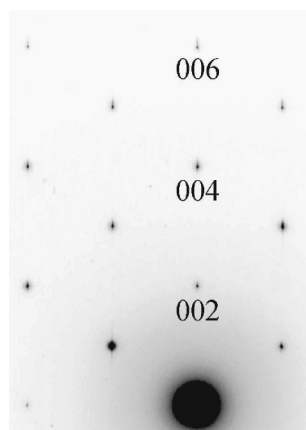


FIG. 13. Electron diffraction pattern of a $40\ \mu\text{m}\times 40\ \mu\text{m}$ island of $\text{Si}_{0.7}\text{Ge}_{0.3}$ (30 nm)/Si (4 nm) on BPSG after 90 min annealing at $820\ ^\circ\text{C}$.

of the Si and SiGe films is identical, which implies that no slip takes place between Si and $\text{Si}_{0.7}\text{Ge}_{0.3}$ as the SiGe relaxes.

IV. SUMMARY

Quantitative analysis of lateral expansion and buckling of compressively strained SiGe islands on a viscous BPSG layer has been carried out. Viscosity of the BPSG is extracted from the lateral expansion. Changing the glass viscosity does not favor either lateral expansion or buckling. Consequently, it cannot be used to suppress buckling. However, use of long annealing times and thicker SiGe films proves to be effective in achieving large flat islands. No dislocations are observed on the relaxed SiGe islands during XTEM experiments, which shows that the relaxation of strained SiGe islands occurs through the compliant BPSG film, and not through dislocation formation.

ACKNOWLEDGMENTS

The authors would like to thank Anthony A. Margarella at Northrop-Grumman in Linthicum, MD, for deposition of the BPSG films. This work is supported by DARPA (N66001-00-1-8957), ARO (DAA655-98-1-0270), and NSF (CMS-9820713).

- ¹Y. H. Lo, *Appl. Phys. Lett.* **59**, 2311 (1991).
- ²K. D. Hobart, F. J. Kub, M. Fatemi, M. E. Twigg, P. E. Thompson, T. S. Kuan, and C. K. Inoki, *J. Electron. Mater.* **29**, 897 (2000).
- ³F. Y. Huang, M. A. Chu, M. O. Tanner, and K. L. Wang, *Appl. Phys. Lett.* **76**, 2680 (2000).
- ⁴N. Sugiyama, T. Mizuno, M. Suzuki, and S. Takagi, *Jpn. J. Appl. Phys., Part 1* **40**, 2875 (2001).
- ⁵Y. H. Luo, J. Wan, R. L. Forrest, J. L. Liu, G. Jin, M. S. Goorsky, and K. L. Wang, *Appl. Phys. Lett.* **78**, 454 (2001).
- ⁶E. A. Fitzgerald, Y.-H. Xie, M. L. Green, D. Brasen, A. R. Kortan, and J. Michel, *Appl. Phys. Lett.* **59**, 811 (1991).
- ⁷M. Fatemi and R. E. Stahlbush, *Appl. Phys. Lett.* **58**, 825 (1991).
- ⁸M. Newberger, *Group IV Semiconducting Materials*, Handbook of Electronic Materials, Vol. 5 (IFI/Plenum, New York, 1971).
- ⁹D. J. Lockwood and J.-M. Baribeau, *Phys. Rev. B* **45**, 8565 (1992).
- ¹⁰J. C. Tsang, P. M. Mooney, F. Dacol, and J. O. Chu, *J. Appl. Phys.* **75**, 8098 (1994).
- ¹¹L. B. Freund and W. D. Nix (unpublished).
- ¹²P. D. Moran and T. F. Kuech, *J. Electron. Mater.* **30**, 802 (2001).
- ¹³R. Huang, H. Yin, J. Liang, K. D. Hobart, J. C. Sturm, and Z. Suo, *Mater. Res. Soc. Symp. Proc.* **695**, 115 (2001).
- ¹⁴N. Sridhar, D. J. Srolovitz, and Z. Suo, *Appl. Phys. Lett.* **78**, 2482 (2001).
- ¹⁵R. Huang and Z. Suo, *J. Appl. Phys.* **91**, 1135 (2002).
- ¹⁶R. Huang and Z. Suo, *Int. J. Solids Struct.* **39**, 1791 (2002).
- ¹⁷N. Sridhar, D. J. Srolovitz, and B. N. Cox, *Acta Mater.* (submitted).
- ¹⁸J. Liang, R. Huang, H. Yin, J. C. Sturm, K. D. Hobart, and Z. Suo, *Acta Mater.* (accepted for publication). (Preprint available online at www.princeton.edu/~suo, Publication 125.)
- ¹⁹M. S. Carroll, J. C. Sturm, and M. Yang, *J. Electrochem. Soc.* **147**, 4652 (2000).